

Computing stability of differential equations with bounded distributed delays

T. Luzyanina, K. Engelborghs, D. Roose

Report TW 340, May 2002



Katholieke Universiteit Leuven
Department of Computer Science

Celestijnenlaan 200A – B-3001 Heverlee (Belgium)

Computing stability of differential equations with bounded distributed delays

T. Luzyanina, K. Engelborghs, D. Roose*

Report TW 340, May 2002

Department of Computer Science, K.U.Leuven

Abstract

This paper concerns stability analysis of scalar delay integro-differential equations (DIDEs). We propose a numerical scheme which involves a linear multistep method as time integration scheme and a quadrature method based on Lagrange interpolation and a Gauss-Legendre quadrature rule. We investigate properties of the proposed scheme with respect to preserving stability properties of the original equation. We derive and prove a sufficient condition for stability of a DIDE (with a constant kernel) which we call RHP-stability. Conditions are obtained under which the proposed quadrature preserves RHP-stability. We compare the obtained results with corresponding ones using Newton-Cotes formulas. Results of numerical experiments on computing stability of DIDEs with constant and non-constant kernel functions are presented.

Keywords : delay integro-differential equations, quadrature rules, numerical stability analysis.

AMS(MOS) Classification : Primary : 65P30, Secondary : 65J15.

*On leave from Institute of Mathematical Problems in Biology, RAS, Pushchino, Moscow region, 142290, Russia

1 Introduction

Differential equations with bounded and continuously distributed delay,

$$\frac{d}{dt}x(t) = f(x(t), \int_{t-\tau_2}^{t-\tau_1} K(t-\xi)g(x(\xi))d\xi), \quad (1.1)$$

are usually called delay integro-differential equations (DIDEs) and, sometimes, functional equations of Volterra type. These equations appear e.g. in modelling population dynamics, the spread of infectious diseases and control theory (see, e.g. [1, 9, 10, 14, 16, 17]). In this paper we restrict ourselves to scalar DIDEs, i.e. $x \in \mathbb{R}$, $f : \mathbb{R} \times \mathbb{R} \rightarrow \mathbb{R}$, $g : \mathbb{R} \rightarrow \mathbb{R}$, and to commensurate (rationally dependent) delays τ_1 and τ_2 . Note that the latter is trivially true when $\tau_1 = 0$. In (1.1), the kernel (weight) function K is defined on the interval $[\tau_1, \tau_2]$, $\tau_2 > \tau_1 \geq 0$.

The local (asymptotic) stability of a steady state solution of a DIDE is studied through the linearization of the original equation around this solution,

$$\frac{d}{dt}y(t) = A_0y(t) + A_1 \int_{t-\tau_2}^{t-\tau_1} K(t-\xi)y(\xi)d\xi, \quad (1.2)$$

where $A_0, A_1 \in \mathbb{R}$. To study the stability of the zero solution of (1.2) with a (general) kernel function $K(\cdot)$, one needs to apply numerical methods. A desirable numerical scheme is one that preserves the stability properties of the continuous problem to which it is applied.

Stability of time integration methods for differential equations with discrete delays (DDEs) has been studied actively during the last decade. This research evolved from a single delay to commensurate delays and further to arbitrary delays and has led to robust numerical methods for stability analysis of DDEs. Numerical treatment of equations with distributed delays is more complicated compared to the case of discrete delays due to the integral terms. In particular, it is known that the kernel function not only affects the stability of solutions but also stability properties of the numerical scheme used. A few results in this direction have appeared.

In [3], the stability properties of a numerical scheme based on a linear multistep (LMS) method and a Newton-Cotes formula approximating (1.2) with $\tau_1 = 0$ and $K(\xi) \equiv 1$, $\xi \in [0, \tau_2]$, are discussed. The authors compare the analytically obtained stability region in the (A_0, A_1) -plane with the one obtained numerically by employing the method of D-partitions and the boundary locus technique (see, e.g. [2]). In [15], the stability of Runge-Kutta methods is studied on the basis of a system of equations similar to (1.2) ($\tau_1 = 0$, $K(\xi) \equiv 1$, $\xi \in [0, \tau_2]$, with an additional delay term, $x(t - \tau_2)$). It is shown that every A -stable Runge-Kutta method preserves the delay-independent stability of the original equation whenever a step size $h = \tau_2/m$ is used, $m \in \mathbb{N}$.

The numerical scheme which we propose in this paper to approximate (1.2) involves an LMS method as time integration scheme and a quadrature method based on Lagrange interpolation and a Gauss-Legendre quadrature rule. The choice of these methods is motivated as follows. The use of LMS methods for stability analysis of systems of DDEs with multiple delays was investigated in [7] and effectively used in [6, 5]. The use of Lagrange interpolation to approximate the delayed variables within an LMS scheme has shown to be efficient with respect to convergence and stability properties of the resulting numerical

scheme (e.g., [11, 7]). Gaussian quadrature rules (“the only all-purpose formulas” [19]) are widely used in applications due to their convergence properties and applicability to integrands having only low-order derivatives.

We derive and prove a sufficient condition for the stability of a DIDE with a constant kernel function, which we call RHP-stability. We investigate stability properties of the proposed numerical scheme with respect to preserving RHP-stability and compare with corresponding results for Newton-Cotes formulas. We show that RHP-stability is preserved, under certain conditions, by the proposed scheme, while it is not preserved when using Newton-Cotes formulas. Even when these conditions are not fulfilled, the proposed scheme remains preferable to Newton-Cotes formulas with respect to preserving stability, as we show numerically. We present results of numerical experiments on computing stability of (1.2) for both constant and non-constant kernel functions.

The paper is structured as follows. In Section 2 we obtain discretized equations approximating (1.2). In Section 3 we consider the stability properties of (1.2) and corresponding discretized versions. We introduce RHP-stability and formulate conditions under which the discretized equation retains the RHP-stability of the original equation. The conditions related to quadrature are further investigated for the proposed quadrature and for Newton-Cotes formulas in Section 4. Results of numerical experiments on computing stability and characteristic roots of (1.2) are given in Section 5. We conclude in Section 6. Appendix A contains the proofs of our theorems.

2 Numerical approximation of equation (1.2)

2.1 Quadrature rules

To approximate the integral in (1.2), we propose a quadrature method based on Lagrange interpolation and Gauss-Legendre quadrature rules. We also formulate Newton-Cotes formulas which we use for comparison.

2.1.1 Proposed quadrature method

Assume that τ_1 and τ_2 are commensurate. Then, let $h > 0$ be a (constant) step size in the discretization of (1.2) such that $\tau_1 = n_1 h$ and $\tau_2 = n_2 h$, $n_1 \in \mathbb{N}$, $n_2 \in \mathbb{N}_0$. Set $n := n_2 - n_1$. Let y_j be the numerical approximation of $y(t)$ at the mesh point $t_j = jh$ (assuming $t_0 = 0$).

The integral in (1.2) can be written in the form

$$\int_{t_j - \tau_2}^{t_j - \tau_1} K(t_j - \xi) y(\xi) d\xi = \sum_{r=1}^n \int_0^h K(q_{1,r} h - \xi) y(t_{j-q_{1,r}} + \xi) d\xi, \quad (2.1)$$

where $q_{1,r} = n_2 - r + 1$. Using $\xi = \epsilon h$, $\epsilon \in [0, 1]$, we approximate the solution $y(t_{j-q_{1,r}} + \xi)$ by the Lagrange interpolation polynomial,

$$y(t_{j-q_{1,r}} + \epsilon h) \simeq \sum_{l=-s_-}^{s_+} P_l(\epsilon) y_{j-q_{1,r}+l}, \quad (2.2)$$

through the points $j - q_{1,r} - s_-, \dots, j - q_{1,r} + s_+$, where s_- respectively s_+ represent the number of interpolation points taken to the left respectively to the right of $t_{j-q_{1,r}}$. The

factors $P_l(\epsilon)$ are the Lagrange coefficients,

$$P_l(\epsilon) := \prod_{\nu=-s_-, \nu \neq l}^{s_+} \frac{\epsilon - \nu}{l - \nu}. \quad (2.3)$$

Then, we substitute (2.2) in (2.1) and apply the m -point Gauss-Legendre quadrature formula (see, e.g. [19]). The result reads

$$\int_{t_j - \tau_2}^{t_j - \tau_1} K(t_j - \xi) y(\xi) d\xi \simeq \sum_{r=1}^n \sum_{k=1}^m B_k K(q_{1,r}h - \epsilon_k h) \sum_{l=-s_-}^{s_+} P_l(\epsilon_k) y_{j-q_{1,r}+l}, \quad (2.4)$$

where $\epsilon_k h$ and B_k are respectively the zeros of the m th-degree Legendre polynomial (Gaussian points) and the weights of the Gauss-Legendre quadrature rule on $[0, h]$. Note that the Gauss-Legendre quadrature rule is exact for the polynomials used whenever $s_- + s_+ \leq 2m - 1$. Below we always assume that the latter holds. For $K(\xi) \equiv 1$, $\xi \in [\tau_1, \tau_2]$, we will use a compact form of (2.4),

$$\int_{t_j - \tau_2}^{t_j - \tau_1} y(\xi) d\xi \simeq \sum_{r=1}^n \sum_{l=-s_-}^{s_+} \omega_l y_{j-q_{1,r}+l}, \quad \omega_l := \sum_{k=1}^m B_k P_l(\epsilon_k). \quad (2.5)$$

We avoid the use of future mesh points in (2.4) and in (2.5) if $s_+ - q_{1,n} \leq 0$, i.e. $\tau_1 \geq (s_+ - 1)h$.

If $\tau_1 < (s_+ - 1)h$, we split the integral (2.1) as

$$\int_{t_j - \tau_2}^{t_j - \tau_1} K(t_j - \xi) y(\xi) d\xi = \int_{t_j - \tau_2}^{t_j - (s_+ - 1)h} K(t_j - \xi) y(\xi) d\xi + \int_{t_j - (s_+ - 1)h}^{t_j - \tau_1} K(t_j - \xi) y(\xi) d\xi. \quad (2.6)$$

Consider the second integral in the right hand side of (2.6),

$$\int_{t_j - (s_+ - 1)h}^{t_j - \tau_1} K(t_j - \xi) y(\xi) d\xi = \sum_{r=1}^{s_+ - 1 - n_1} \int_0^h K(q_{2,r}h - \xi) y(t_{j-q_{2,r}} + \xi) d\xi, \quad (2.7)$$

where $q_{2,r} = s_+ - r$. Since $q_{2,r} < s_+$, we approximate the solution $y(t_{j-q_{2,r}} + \xi)$, using $\xi = \epsilon h$, $\epsilon \in [0, 1]$, by the following Lagrange interpolation polynomial of degree $s_- + s_+$,

$$y(t_{j-q_{2,r}} + \epsilon h) \simeq \sum_{l=-s(r)_-}^{s(r)_+} P_{l,r}(\epsilon) y_{j-q_{2,r}+l}, \quad s(r)_- := s_- + r, \quad s(r)_+ := s_+ - r, \quad (2.8)$$

through the points $j - q_{2,r} - s(r)_-, \dots, j - q_{2,r} + s(r)_+$. The factors $P_{l,r}(\epsilon)$ are the Lagrange coefficients,

$$P_{l,r}(\epsilon) = \prod_{\nu=-s(r)_-, \nu \neq l}^{s(r)_+} \frac{\epsilon - \nu}{l - \nu}. \quad (2.9)$$

Note the difference in interpolation formulas (2.2) and (2.8): in the latter case the interpolation has a rather ‘‘one side’’ nature. For example, when $\tau_1 = 0$, the solution $y(t_{j-1} + \xi)$ is approximated using the solution at points $j - s_- - s_+, \dots, j$.

After substitution of (2.8) in (2.7) and applying the m -point Gauss-Legendre quadrature rule (also with $2m - 1 \geq s_- + s_+$), the result reads

$$\int_{t_j - (s_+ - 1)h}^{t_j - \tau_1} K(t_j - \xi)y(\xi)d\xi \simeq \sum_{r=1}^{s_+ - 1 - n_1} \sum_{k=1}^m B_k K(q_{2,r}h - \epsilon_k h) \sum_{l=-s(r)_-}^{s(r)_+} P_{l,r}(\epsilon_k)y_{j-q_{2,r}+l}, \quad (2.10)$$

and, for $K(\xi) \equiv 1$, $\xi \in [\tau_1, \tau_2]$,

$$\int_{t_j - (s_+ - 1)h}^{t_j - \tau_1} y(\xi)d\xi \simeq \sum_{r=1}^{s_+ - 1 - n_1} \sum_{l=-s(r)_-}^{s(r)_+} \omega_{l,r} y_{j-q_{2,r}+l}, \quad \omega_{l,r} := \sum_{k=1}^m B_k P_{l,r}(\epsilon_k). \quad (2.11)$$

2.1.2 Newton-Cotes formulas

Let m ($m \geq 2$) and ω_l ($l = 1, \dots, m$) be the number of points, respectively weights used in a Newton-Cotes formula (see, e.g. [12]). For a fixed m , let h , the step size of discretization of (1.2), be such that we could use the m -point repeated Newton-Cotes rule on the interval of integration, i.e. $\tau_2 - \tau_1 = n_m(m-1)h$, $\tau_1 = n_{1,m}h$, $\tau_2 = n_{2,m}h$, $n_{1,m} \in \mathbb{N}$, $n_m, n_{2,m} \in \mathbb{N}_0$. Set $h_m := (m-1)h$. The m -point Newton-Cotes formula applied to the integral in (1.2) then leads to

$$\begin{aligned} \int_{t_j - \tau_2}^{t_j - \tau_1} K(t_j - \xi)y(\xi)d\xi &= \sum_{r=1}^{n_m} \int_0^{h_m} K(q_r h - \xi)y(t_j - q_r h + \xi)d\xi \\ &\simeq \sum_{r=1}^{n_m} \sum_{l=1}^m \omega_l K((q_r - l + 1)h)y_{j-q_r+l-1}, \end{aligned} \quad (2.12)$$

where $q_r = n_{2,m} - (r-1)(m-1)$ and the weights ω_l , $l = 1, \dots, m$, are defined on the interval $[0, h_m]$.

Note that for the trapezoidal rule $m = 2$ and $\omega_1 = \omega_2 = h/2$. For a constant kernel function, this rule is equivalent to the 2-point Gauss-Legendre quadrature rule (2.5) with $s_- = 0$, $s_+ = 1$ since $P_0(\epsilon_1) + P_0(\epsilon_2) = P_1(\epsilon_1) + P_1(\epsilon_2) = 1$ and $B_1 = B_2 = h/2$.

2.2 Quadrature within an LMS scheme

For time integration of (1.2), we apply a linear k -step (consistent and irreducible) formula (see, e.g. [8]) coupled with the proposed quadrature. The result reads

$$\begin{aligned} \sum_{j=0}^k \alpha_j y_{u+j} &= h \sum_{j=0}^k \beta_j (A_0 y_{u+j} \\ &+ A_1 (\sum_{r=1}^{n_c} \sum_{i=1}^m B_i K(q_{1,r}h - \epsilon_i h) \sum_{l=-s_-}^{s_+} P_{l,i}(\epsilon_i) y_{u+j-q_{1,r}+l} \\ &+ \sum_{r=1}^{n_s} \sum_{i=1}^m B_i K(q_{2,r}h - \epsilon_i h) \sum_{l=-s(r)_-}^{s(r)_+} P_{l,i}(\epsilon_i) y_{u+j-q_{2,r}+l})), \end{aligned} \quad (2.13)$$

where α_j , β_j are the coefficients of the LMS method, $n_c = n$, $n_s = 0$ if $\tau_1 \geq (s_+ - 1)h$ and $n_c = n_2 - s_+ + 1$, $n_s = s_+ - 1 - n_1$ otherwise.

Similarly, the use of the m -point Newton-Cotes formula within an LMS scheme leads to

$$\sum_{j=0}^k \alpha_j y_{u+j} = h \sum_{j=0}^k \beta_j (A_0 y_{u+j} + A_1 (\sum_{r=1}^{n_m} \sum_{l=1}^m \omega_l K((q_r - l + 1)h) y_{u+j-q_r+l-1})). \quad (2.14)$$

All notations in (2.13) and (2.14) are defined as in sections 2.1.1 respectively 2.1.2. Note that during time integration the discretized equation is solved for y_{u+k} based on the previously computed y_{u+j} , $j < k$, and an initial condition.

3 Asymptotic stability of equation (1.2) and its numerical approximations

For the definition of asymptotic stability of a DIDE of the form (1.2) and its numerical approximation we refer to [3]. The following results give conditions for stability.

Equation (1.2) is asymptotically stable (equivalently, the zero solution of (1.2) is asymptotically stable) if and only if all the zeros (characteristic roots) of the characteristic equation

$$\lambda = A_0 + A_1 \int_{\tau_1}^{\tau_2} K(\xi) e^{-\lambda \xi} d\xi \quad (3.1)$$

have negative real part (see, e.g. [9, 3]). There exist an infinite number of roots $\lambda \in \mathbb{C}$ of (3.1) and the number of roots in any right half plane $\Re(\lambda) > \eta$, $\eta \in \mathbb{R}$, is finite [9]. Hence, the stability is always defined by a finite number of roots, as in the case of differential equations with discrete delays.

The discretized equation (2.13) is strictly stable (equivalently, its zero solution is strictly stable) if and only if the characteristic equation

$$\begin{aligned} \frac{1}{h} \left(\frac{\sum_{j=0}^k \alpha_j \mu^j}{\sum_{j=0}^k \beta_j \mu^j} \right) &= A_0 + A_1 \left(\sum_{r=1}^{n_c} \sum_{i=1}^m B_i K(q_{1,r} h - \epsilon_i h) \sum_{l=-s_-}^{s_+} P_l(\epsilon_i) \mu^{-(q_{1,r}-l)} \right. \\ &\quad \left. + \sum_{r=1}^{n_s} \sum_{i=1}^m B_i K(q_{2,r} h - \epsilon_i h) \sum_{l=-s(r)_-}^{s(r)_+} P_{l,r}(\epsilon_i) \mu^{-(q_{2,r}-l)} \right) \end{aligned} \quad (3.2)$$

has all its roots μ in the open disk $|\mu| < 1$ (see, e.g. [3]).

To compare the roots μ of (3.2) with the solutions λ of the characteristic equation (3.1), we use the relation $\mu = \exp(\lambda h)$ and we set

$$\text{LMS}(\lambda h) := \frac{\sum_{j=0}^k \alpha_j e^{\lambda h j}}{\sum_{j=0}^k \beta_j e^{\lambda h j}}.$$

Then (3.2) is equivalent to

$$\begin{aligned} \frac{1}{h} \text{LMS}(\lambda h) &= A_0 + A_1 \left(\sum_{r=1}^{n_c} \sum_{i=1}^m B_i K(q_{1,r} h - \epsilon_i h) \sum_{l=-s_-}^{s_+} P_l(\epsilon_i) e^{-\lambda h (q_{1,r}-l)} \right. \\ &\quad \left. + \sum_{r=1}^{n_s} \sum_{i=1}^m B_i K(q_{2,r} h - \epsilon_i h) \sum_{l=-s(r)_-}^{s(r)_+} P_{l,r}(\epsilon_i) e^{-\lambda h (q_{2,r}-l)} \right). \end{aligned} \quad (3.3)$$

By the requirement of irreducibility and the fact that solutions $\mu = 0$ do not influence stability, it follows that the stability of the discretized equation is now determined by the real parts of the (finite number of) solutions λ of (3.3) just as for the characteristic equation (3.1).

In the next section we investigate properties of quadrature rules in case of a constant kernel function. Therefore, we now assume $K(\xi) \equiv 1$, $\xi \in [\tau_1, \tau_2]$. The stability of equation (1.2) with non-constant kernel functions is considered in section 5.

We consider the characteristic equations

$$\lambda = A_0 + A_1 \int_{\tau_1}^{\tau_2} e^{-\lambda\xi} d\xi, \quad (3.4)$$

and

$$\frac{1}{h} \text{LMS}(\lambda h) = A_0 + A_1 \left(\sum_{r=1}^{n_c} \sum_{l=-s_-}^{s_+} \omega_l e^{-\lambda h(q_{1,r-l})} + \sum_{r=1}^{n_s} \sum_{l=-s(r)_-}^{s(r)_+} \omega_{l,r} e^{-\lambda h(q_{2,r-l})} \right). \quad (3.5)$$

Let \mathbb{C}_0^+ , \mathbb{C}^+ denote the open respectively closed right half plane,

$$\mathbb{C}_0^+ = \{\lambda \in \mathbb{C} \mid \Re(\lambda) > 0\} \text{ and } \mathbb{C}^+ = \{\lambda \in \mathbb{C} \mid \Re(\lambda) \geq 0\},$$

and \mathbb{C}_0^- , \mathbb{C}^- denote the open respectively closed left half plane (with corresponding definitions). We define the set-valued functions $\Sigma_c(\cdot)$ and $\Sigma_{ch}(\cdot)$ as

$$\Sigma_c(C) = \bigcup_{\lambda \in C} (A_0 + A_1 \int_{\tau_1}^{\tau_2} e^{-\lambda\xi} d\xi), \quad C \subset \mathbb{C}, \quad (3.6a)$$

$$\Sigma_{ch}(C) = \bigcup_{\lambda \in C} (A_0 + A_1 \left(\sum_{r=1}^{n_c} \sum_{l=-s_-}^{s_+} \omega_l e^{-\lambda h(q_{1,r-l})} + \sum_{r=1}^{n_s} \sum_{l=-s(r)_-}^{s(r)_+} \omega_{l,r} e^{-\lambda h(q_{2,r-l})} \right)). \quad (3.6b)$$

In the context of stability analysis, the mapping of \mathbb{C}^+ under Σ_c and Σ_{ch} , i.e. the sets $\Sigma_c(\mathbb{C}^+)$ and $\Sigma_{ch}(\mathbb{C}^+)$, is of interest. Note that these sets are bounded subsets of \mathbb{C} because

$$\begin{aligned} \tilde{\lambda} \in \Sigma_c(\mathbb{C}^+) &\Rightarrow |\tilde{\lambda} - A_0| \leq |A_1| (e^{-\lambda\tau_1} - e^{-\lambda\tau_2}) / \lambda \leq |A_1| (\tau_2 - \tau_1), \quad \lambda \in \mathbb{C}^+, \\ \tilde{\lambda} \in \Sigma_{ch}(\mathbb{C}^+) &\Rightarrow |\tilde{\lambda} - A_0| \leq |A_1| (n_c h + n_s h) = |A_1| (\tau_2 - \tau_1). \end{aligned} \quad (3.7)$$

The latter holds because $q_{1,r} - s_+ \geq 0$, $r = 1, \dots, n_c$, $\sum_{l=-s_-}^{s_+} \omega_l = h$ and $q_{2,r} - s(r)_+ = 0$, $\sum_{l=-s(r)_-}^{s(r)_+} \omega_{l,r} = h$, $r = 1, \dots, n_s$. It follows from (3.7) that the mapping of \mathbb{C}^+ under Σ_c and Σ_{ch} is inside a circle centered at A_0 with radius $|A_1|(\tau_2 - \tau_1)$.

The condition

$$\Sigma_c(\mathbb{C}^+) \subset \mathbb{C}_0^- \quad (3.8)$$

is a sufficient condition for stability of (3.4). Indeed, it implies that the right hand side of (3.4) maps the right half plane (RHP) $\Re(\lambda) \geq 0$ into the left half plane. Hence (3.4) cannot have solutions with positive real part. We will refer to (3.8) as RHP-stability. Obviously, the condition

$$A_0 + |A_1|(\tau_2 - \tau_1) < 0 \quad (3.9)$$

is a sufficient condition for RHP-stability.

We will call the region $\mathbb{C} \setminus \text{LMS}(\mathbb{C}^+)$ the stability region of the corresponding LMS method [8]. It is the region into which $\text{LMS}(\cdot)$ does not map any unstable λ , $\Re(\lambda) \geq 0$. If

$$\Sigma_c(\mathbb{C}^+) \subset \frac{1}{h} (\mathbb{C} \setminus \text{LMS}(\mathbb{C}^+)) \quad (3.10a)$$

and

$$\Sigma_{ch}(\mathbb{C}^+) \subseteq \Sigma_c(\mathbb{C}^+), \quad (3.10b)$$

then the RHP-stability is recovered by the numerical scheme.

If $\mathbb{C} \setminus \text{LMS}(\mathbb{C}^+)$ contains a semicircle of radius ρ_{LMS} , then one can assure condition (3.10a) by an appropriate choice of the step size h ,

$$h < \frac{\rho_{\text{LMS}}}{|A_0| + |A_1|(\tau_2 - \tau_1)}. \quad (3.11)$$

Note that such a semicircle exists, for instance, for all backward differentiation methods.

Condition (3.10b) is equivalent to the condition

$$\Sigma_h(\tau_1, \tau_2; \mathbb{C}^+) \subseteq \Sigma(\tau_1, \tau_2; \mathbb{C}^+), \quad (3.12)$$

which we study in the next section. Here the set-valued function $\Sigma(\cdot, \cdot; \cdot)$ is defined as

$$\Sigma(\tau_1, \tau_2; C) = \bigcup_{\lambda \in C} \left(\int_{\tau_1}^{\tau_2} e^{-\lambda \xi} d\xi \right), \quad C \subset \mathbb{C},$$

and $\Sigma_h(\cdot, \cdot; \cdot)$ is its discrete analogue. The equivalence of (3.10b) and (3.12) is because A_0 and A_1 represent a translation respectively scaling of the mapping. To distinguish between quadratures, we will replace the notation Σ_h by $\Sigma_{h, GL}$ for the proposed quadrature and by $\Sigma_{h, NC}$ for Newton Cotes formulas. So,

$$\Sigma_{h, GL}(\tau_1, \tau_2; C) = \bigcup_{\lambda \in C} \left(\sum_{r=1}^{n_c} \sum_{l=-s_-}^{s_+} \omega_l e^{-\lambda h(q_{1,r-l})} + \sum_{r=1}^{n_s} \sum_{l=-s(r)_-}^{s(r)_+} \omega_{l,r} e^{-\lambda h(q_{2,r-l})} \right), \quad (3.13)$$

$$\Sigma_{h, NC}(\tau_1, \tau_2; C) = \bigcup_{\lambda \in C} \left(\sum_{r=1}^{n_m} \sum_{l=1}^m \omega_l e^{-\lambda h(q_r - l + 1)} \right), \quad C \subset \mathbb{C}. \quad (3.14)$$

Note that $\Sigma_{h, NC}(\tau_1, \tau_2; \mathbb{C}^+)$ was obtained by using a similar analysis for the discretized equation (2.14) with $K = 1$. Clearly, $\Sigma(\tau_1, \tau_2; \mathbb{C}^+)$, $\Sigma_{h, GL}(\tau_1, \tau_2; \mathbb{C}^+)$ and $\Sigma_{h, NC}(\tau_1, \tau_2; \mathbb{C}^+)$ are bounded subsets of \mathbb{C} .

We need the following results related to (3.12).

Theorem 3.1 *The region defined by $\Sigma(\tau_1, \tau_2; \mathbb{C}^+)$ is located inside the curve $\Sigma(\tau_1, \tau_2; \bigcup_{\theta \in \mathbb{R}} i\theta)$.*

Due to this theorem, RHP-stability (3.8) is equivalent to the condition

$$\Re\left(A_0 + A_1 \frac{e^{-i\tau_1\theta} - e^{-i\tau_2\theta}}{i\theta}\right) < 0 \quad \text{for all } \theta \in \mathbb{R}, \quad (3.15)$$

which implies that for analyzing stability it is sufficient to examine the mapping of the imaginary axis under Σ_c . Obviously, if (3.15) holds for certain values of A_0 , A_1 , τ_1 and τ_2 , then it also holds for A_0 , A_1/ρ , $\tau_1\rho$, $\tau_2\rho$, with $\rho > 0$. Hence RHP-stability is independent of the factor ρ .

The next two theorems are analogous to theorem 3.1.

Theorem 3.2 *The region defined by $\Sigma_{h, GL}(\tau_1, \tau_2; \mathbb{C}^+)$ is located inside the curve $\Sigma_{h, GL}(\tau_1, \tau_2; \bigcup_{\theta \in \mathbb{R}} i\theta)$.*

Theorem 3.3 *The region defined by $\Sigma_{h, NC}(\tau_1, \tau_2; \mathbb{C}^+)$ is located inside the curve $\Sigma_{h, NC}(\tau_1, \tau_2; \bigcup_{\theta \in \mathbb{R}} i\theta)$.*

In the next section we investigate whether condition (3.12) is fulfilled for the proposed quadrature scheme and for Newton-Cotes formulas.

4 Properties of quadrature rules for a constant kernel

4.1 Proposed quadrature method

Our study has shown that Lagrange interpolation which we use when $\tau_1 \geq (s_+ - 1)h$ and $\tau_1 < (s_+ - 1)h$, cf. (2.2) respectively (2.8), affects the properties of the proposed quadrature scheme. Therefore, we consider these two cases separately.

- Case $\tau_1 \geq (s_+ - 1)h$.

Note that $\tau_1 = 0$ implies $s_+ \leq 1$. It follows from (3.13), using $n_c = n$ and $n_s = 0$ (i.e. $\tau_1 \geq (s_+ - 1)h$), that

$$\Sigma_{h,GL}(\tau_1, \tau_2; C) = \bigcup_{\lambda \in C} (e^{-\lambda\tau_1} \sum_{r=1}^n e^{-\lambda h(r-1)} \sum_{l=-s_-}^{s_+} \omega_l e^{\lambda h(l-1)}). \quad (4.1)$$

To determine the location of $\Sigma_{h,GL}(\tau_1, \tau_2; \mathbb{C}^+)$ w.r.t. $\Sigma(\tau_1, \tau_2; \mathbb{C}^+)$, we first obtain some preliminary results. Let

$$\partial\Sigma(0, h) := \Sigma(0, h; \bigcup_{\theta \in [-2\pi/h, 2\pi/h]} i\theta) \quad \text{and} \quad \partial\Sigma_{h,GL}(0, h) := \Sigma_{h,GL}(0, h; \bigcup_{\theta \in [-\pi/h, \pi/h]} i\theta).$$

Lemma 4.1 $\Sigma(0, h; \bigcup_{\theta \in \mathbb{R}} i\theta)$ is bounded by the closed curve $\partial\Sigma(0, h)$. $\Sigma_{h,GL}(0, h; \bigcup_{\theta \in \mathbb{R}} i\theta)$ is equivalent to the closed curve $\partial\Sigma_{h,GL}(0, h)$.

Theorem 4.1 If $s_+ = s_- + 1$, then the curve $\partial\Sigma_{h,GL}(0, h)$ is inside the curve $\partial\Sigma(0, h)$.

Corollary 4.1 If $\tau_1 \geq (s_+ - 1)h$ and $s_+ = s_- + 1$, then the curve $\Sigma_{h,GL}(\tau_1, \tau_2; \bigcup_{\theta \in \mathbb{R}} i\theta)$ is inside the curve $\Sigma(\tau_1, \tau_2; \bigcup_{\theta \in \mathbb{R}} i\theta)$.

Note that the conditions of the corollary are equivalent to the following conditions on the Lagrange interpolation: $s_- \leq \tau_1/h$, $s_+ = s_- + 1$. Obviously, when $\tau_1 = 0$, the conditions are only satisfied if $s_- = 0$ and $s_+ = 1$.

The following theorem follows from theorems 3.1, 3.2, corollary 4.1 and gives conditions under which (3.12) is fulfilled.

Theorem 4.2 If $s_- \leq \tau_1/h$ and $s_+ = s_- + 1$, then $\Sigma_{h,GL}(\tau_1, \tau_2; \mathbb{C}^+) \subseteq \Sigma(\tau_1, \tau_2; \mathbb{C}^+)$.

The results of theorem 4.1 and corollary 4.1 (and hence theorem 4.2) are illustrated in fig. 1. Note that in all figures we use notations $\partial\Sigma(\cdot, \cdot)$ and $\partial\Sigma_{h,GL}(\cdot, \cdot)$ for the boundaries of $\Sigma(\cdot, \cdot; \bigcup_{\theta \in \mathbb{R}} i\theta)$ respectively $\Sigma_{h,GL}(\cdot, \cdot; \bigcup_{\theta \in \mathbb{R}} i\theta)$.

- Case $\tau_1 < (s_+ - 1)h$.

We will assume that $s_+ = s_- + 1$ (hence $\tau_1 < s_-h$) and that $s_- > n_1$ (since $s_- \leq n_1 \Rightarrow \tau_1 \geq s_-h$). It follows from (3.13), using $n_c = n_2 - s_-$ and $n_s = s_- - n_1$, that

$$\begin{aligned} \Sigma_{h,GL}(\tau_1, \tau_2; C) = & \bigcup_{\lambda \in C} (e^{-\lambda h s_-} \sum_{r=1}^{n_2 - s_-} e^{-\lambda h(r-1)} \sum_{l=-s_-}^{s_+} \omega_l e^{\lambda h(l-1)} \\ & + \sum_{r=1}^{s_- - n_1} e^{-\lambda h(s_+ - r)} \sum_{l=-s(r)_-}^{s(r)_+} \omega_{l,r} e^{\lambda h l}). \end{aligned} \quad (4.2)$$

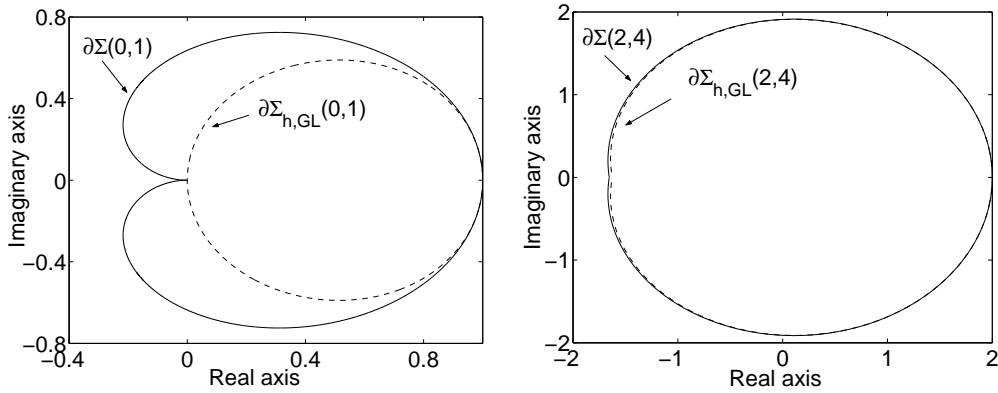


Figure 1: Solid and dashed lines denote the boundary curves $\partial\Sigma$ respectively $\partial\Sigma_{h,GL}$. Left: $\partial\Sigma(0, h)$ and $\partial\Sigma_{h,GL}(0, h)$. Right: $\partial\Sigma(\tau_1, \tau_2)$ and $\partial\Sigma_{h,GL}(\tau_1, \tau_2)$. $h = 1$, $\tau_1 = 2$, $\tau_2 = 4$, $s_- = 1$, $s_+ = 2$.

Numerical experiments have shown that whether or not $\Sigma_{h,GL}(\tau_1, \tau_2; \mathbb{C}^+)$ is a subset of $\Sigma(\tau_1, \tau_2; \mathbb{C}^+)$ depends on the values τ_1 , τ_2 , s_- (assuming $s_+ = s_- + 1$) and h and that in most cases $\Sigma_{h,GL}(\tau_1, \tau_2; \mathbb{C}^+) \not\subset \Sigma(\tau_1, \tau_2; \mathbb{C}^+)$. Below we give some analysis.

When $\tau_2 = s_- h$ (i.e. $n_2 = s_-$), the first of the two terms in (4.2) is absent and we consider sets $\Sigma(\tau_1, s_- h; \mathbb{C}^+)$ and $\Sigma_{h,GL}(\tau_1, s_- h; \mathbb{C}^+)$. Figure 2, where boundaries of these sets are shown for $\tau_1 \neq 0$ and $\tau_1 = 0$, suggests that the boundary of $\Sigma_{h,GL}(\tau_1, \tau_2; \mathbb{C}^+)$ can closely approximate the boundary of $\Sigma(\tau_1, \tau_2; \mathbb{C}^+)$ when $\tau_1 \neq 0$. The corresponding results are shown in fig. 3 for $\tau_2 > s_- h$ and $\tau_1 \neq 0$. Here an enlargement of the left parts (i.e. the most illustrative parts) of the boundaries of $\Sigma_{h,GL}$ and Σ is depicted for different values of τ_1 , τ_2 and s_- . If $\tau_1 = 0$, then $\Sigma_{h,GL}(0, \tau_2; \mathbb{C}^+) \not\subset \Sigma(0, \tau_2; \mathbb{C}^+)$ for any values of τ_2 , cf. fig. 4. Note that the size of the external part of $\Sigma_{h,GL}(0, \tau_2; \mathbb{C}^+)$ with respect to $\Sigma(0, \tau_2; \mathbb{C}^+)$ decreases with h .

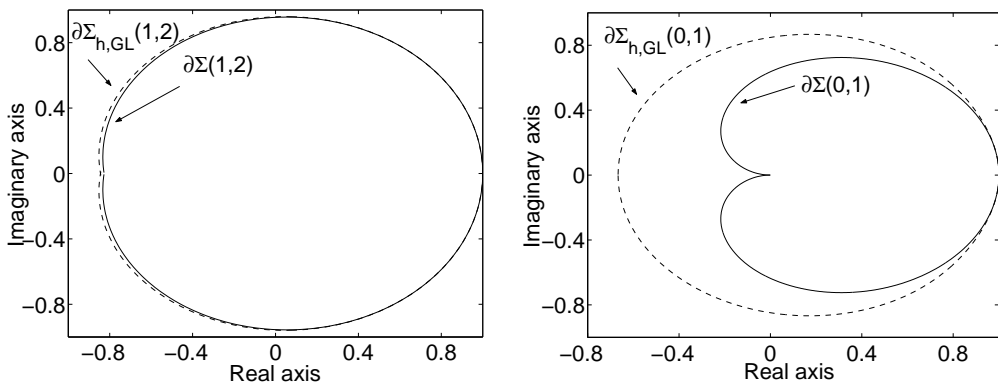


Figure 2: Boundaries of $\Sigma(\tau_1, s_- h; \mathbb{C}^+)$ and $\Sigma_{h,GL}(\tau_1, s_- h; \mathbb{C}^+)$ are denoted by solid respectively dashed lines. Left: $h = 1$, $\tau_1 = 1$, $s_- = 2$. Right: $h = 1$, $\tau_1 = 0$, $s_- = 1$.

We conclude that the proposed quadrature method assures the condition (3.12) for any h (satisfying $\tau_1 = n_1 h$, $\tau_2 = n_2 h$) under the following conditions on the Lagrange interpolation: $s_- \leq \tau_1/h$ and $s_+ = s_- + 1$. If $\tau_1 \neq 0$, the first condition can be satisfied by choosing $h \leq \tau_1/s_-$ for a given s_- . If $\tau_1 = 0$, then (3.12) is only satisfied by using the

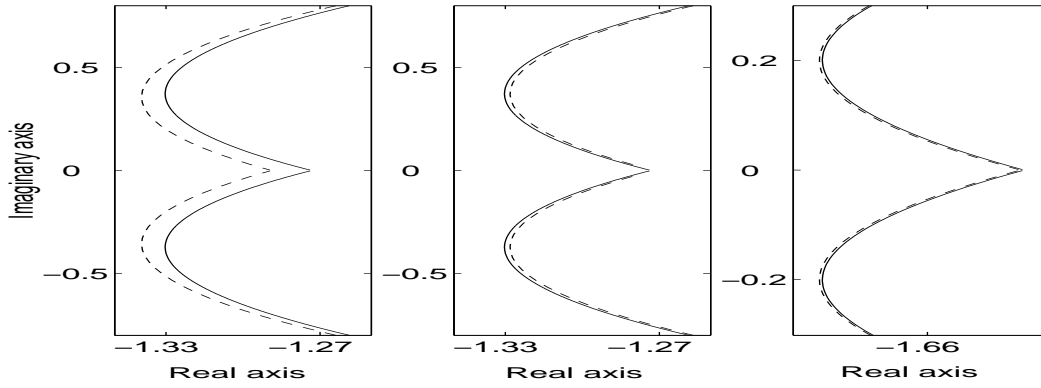


Figure 3: Parts of the boundaries of $\Sigma(\tau_1, \tau_2; \mathbb{C}^+)$ (solid line) and $\Sigma_{h, GL}(\tau_1, \tau_2; \mathbb{C}^+)$ (dashed line). Left: $h = 1$, $\tau_1 = 1$, $\tau_2 = 3$, $s_- = 2$. Middle: $h = 1$, $\tau_1 = 1$, $\tau_2 = 4$, $s_- = 2$. Right: $h = 1$, $\tau_1 = 2$, $\tau_2 = 4$, $s_- = 3$.

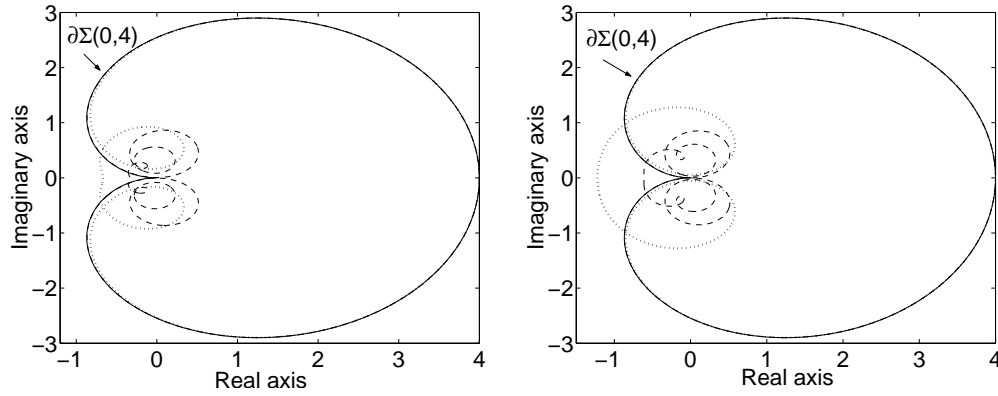


Figure 4: $\partial\Sigma(0, \tau_2)$ and $\Sigma_{h, GL}(0, \tau_2; \bigcup_{\theta \in \mathbb{R}} i\theta)$ are denoted by solid respectively dotted ($h = 1$) and dashed ($h = 0.5$) lines. $\tau_2 = 4$. Left: $s_- = 1$. Right: $s_- = 2$.

Lagrange polynomial of degree 1, i.e. $s_- = 0$, $s_+ = 1$ (equivalently, using the trapezoidal rule).

It is interesting to note that in an LMS-approximation of DDEs coupled with Lagrange interpolation for delayed solution terms, the condition $s_- \leq s_+ \leq s_- + 2$ is used to retain the stability of the original equation (see, e.g. [11, 7]). Our numerical experiments showed that theorem 4.1 holds for $s_+ = s_- + 2$. However, theorem 4.2 does not hold both for $s_+ = s_-$ and for $s_+ = s_- + 2$.

4.2 Newton-Cotes formulas

For m -point Newton-Cotes formulas with $m \geq 3$, numerical experiments showed that $\Sigma_{h, NC}(\tau_1, \tau_2; \mathbb{C}^+) \not\subset \Sigma(\tau_1, \tau_2; \mathbb{C}^+)$ for any values of τ_1 and τ_2 , see figs. 5 and 6. Moreover, when $\tau_1 = 0$, the size of the external part of $\Sigma_{h, NC}(0, \tau_2; \mathbb{C}^+)$ with respect to $\Sigma(0, \tau_2; \mathbb{C}^+)$ does not decrease significantly with h in contrast to the situation with the proposed quadrature scheme (compare figs. 4 and 6). The latter is due to the following property of Newton-Cotes formulas.

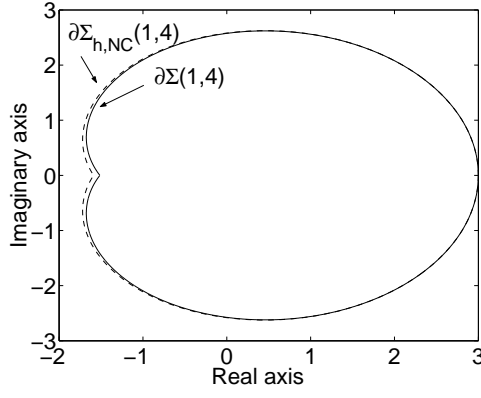


Figure 5: Solid and dashed lines denote $\partial\Sigma(\tau_1, \tau_2)$ respectively $\partial\Sigma_{h,NC}(\tau_1, \tau_2)$, $\tau_1 = 1$, $\tau_2 = 4$, $h = 1$, $m = 4$. Here $\partial\Sigma_{h,NC}(\cdot, \cdot)$ denotes the boundary of $\Sigma_{h,NC}(\cdot, \cdot; \bigcup_{\theta \in \mathbb{R}} i\theta)$.

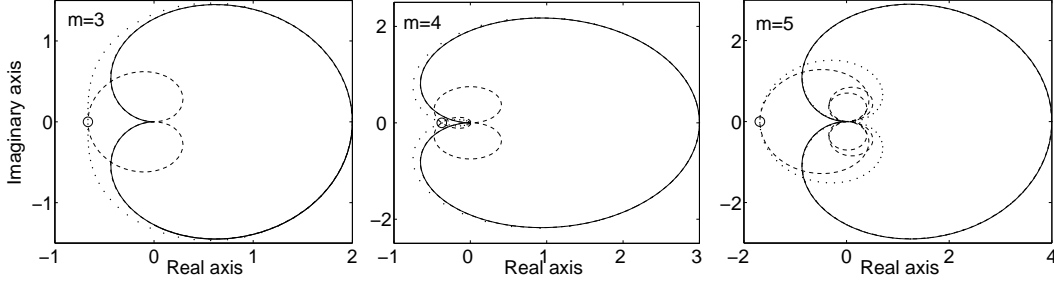


Figure 6: $\partial\Sigma(0, h_m)$ and $\Sigma_{h,NC}(0, h_m; \bigcup_{\theta \in \mathbb{R}} i\theta)$ are denoted by solid respectively dotted ($h = 1$) and dashed ($h = 0.5$) lines. $h_m = (m - 1)h$, $m = 3, 4, 5$. Points M_m are denoted by \circ .

Let

$$S_h(\tau_1, \tau_2; \theta) := \sum_{r=1}^{n_m} \sum_{l=1}^m \omega_l e^{-i\theta h(g_r - l + 1)} = e^{-i\theta \tau_1} \sum_{r=1}^{n_m} e^{-i\theta h(r-1)(m-1)} \sum_{l=1}^m \omega_l e^{i\theta h(l-m)}, \quad \theta \in \mathbb{R}. \quad (4.3)$$

Obviously, $\bigcup_{\theta \in \mathbb{R}} S_h(\tau_1, \tau_2; \theta) = \Sigma_{h,NC}(\tau_1, \tau_2; \bigcup_{\theta \in \mathbb{R}} i\theta)$, where $\Sigma_{h,NC}$ is defined by (3.14).

Let $M_m := \max_{\theta^*} |\Re(S_h(0, h_m; \theta^*))|$, where θ^* is such that $\Re(S_h(0, h_m; \theta^*)) < 0$ and $\Im(S_h(0, h_m; \theta^*)) = 0$, see fig. 6. We will show that M_m does not depend on h . Let $\tilde{m} := \lfloor \frac{m}{2} \rfloor$. Since $\omega_l = \omega_{m-l+1}$, $l = 1, \dots, \tilde{m}$, we obtain

$$\begin{aligned} S_h(0, h_m; \theta) &= e^{i\theta h \frac{1-m}{2}} \left(\sum_{l=1}^{\tilde{m}} \omega_l (e^{i\theta h(l - \frac{m+1}{2})} + e^{-i\theta h(l - \frac{m+1}{2})}) + k\omega_{\tilde{m}+1} \right) \\ &= e^{i\theta h \frac{1-m}{2}} Q, \quad Q := \sum_{l=1}^{\tilde{m}} 2\omega_l \cos(\theta h(l - (m+1)/2)) + k\omega_{\tilde{m}+1} \in \mathbb{R}, \end{aligned} \quad (4.4)$$

where $k = 0$ if m is even and $k = 1$ otherwise. Hence $\Im(S_h(0, h_m; \theta_j^*)) = 0$ for $\theta_j^* = 2\pi j / (1-m)h$, $j = 1, 2, \dots$. We halve the stepsize h and define $\tilde{h} := h/2$, $\tilde{h}_m := h_m/2$ and $\tilde{\omega}_l := \omega_l/2$. Using (4.3) and $n_m = h_m/\tilde{h}_m = 2$, we have

$$S_h(0, h_m; \theta) = (1 + e^{-i\theta \tilde{h}(m-1)}) \tilde{S}_h(0, \tilde{h}_m; \theta), \quad (4.5)$$

where $\tilde{S}_h(0, \tilde{h}_m; \theta)$ is defined similar to (4.4) using $\tilde{\omega}_l$ and \tilde{h} instead of ω_l respectively h . Hence $\Im(\tilde{S}_h(0, \tilde{h}_m; 2\theta_j^*)) = 0$ and $\Re(\tilde{S}_h(0, \tilde{h}_m; 2\theta_j^*)) = \Re(S_h(0, h_m; \theta_j^*)) / 2$. It follows from

(4.5) that $\Re(S_h(0, h_m; 2\theta_j^*)) = 2\Re(\tilde{S}_h(0, \tilde{h}_m; 2\theta_j^*))$. As a consequence, M_m remains constant when changing h . Some examples ($M_3 = -2/3$, $M_4 = -3/8$, $M_5 = -76/45$) are depicted in fig. 6.

5 Numerical experiments

In this section we present results of numerical experiments on computing the stability of the zero solution of equation (1.2) with constant and non-constant kernel functions $K(\cdot)$. We select such functions $K(\xi)$ that, combined with the exponential function $e^{\lambda\xi}$, allow analytical integration and hence allow to obtain “exact” characteristic roots of (3.1) which can be compared with their numerical approximations.

In order to compute roots of the characteristic equation (3.3), we compute the eigenvalues μ of the (linear) map between $[y_{u-L} \ y_{u-L+1} \cdots y_{u+k-1}]$ and $[y_{u-L+1} \ y_{u-L+2} \cdots y_{u+k}]$ using the numerical scheme (2.13) for y_{u+k} and a shift for all other variables (here $L := n_2 + s_-$). Since (2.13) defines an approximation of the time integration operator over the time step h , the eigenvalues μ approximate the eigenvalues of this operator which are exponential transform of the roots λ of the characteristic equation (3.1). Let λ^h denote the characteristic roots of (3.3), to avoid confusing with roots λ of (3.1). Hence, once μ is computed, λ^h can be extracted using $\mu = e^{\lambda^h h}$ [7]:

$$\Re(\lambda^h) = \frac{\ln(|\mu|)}{h}, \quad \Im(\lambda^h) = \frac{\arcsin\left(\frac{\Im(\mu)}{|\mu|}\right)}{h} \pmod{\frac{\pi}{h}}.$$

5.1 Constant kernel function

First we illustrate how violation of condition (3.12), i.e. $\Sigma_h(\tau_1, \tau_2; \mathbb{C}^+) \not\subseteq \Sigma(\tau_1, \tau_2; \mathbb{C}^+)$, may influence the preservation of the RHP-stability of (1.2) by a numerical scheme. Then, using the proposed quadrature method, we present results on the convergence orders of the numerical approximations to the rightmost roots of the characteristic equation (3.4).

For the first purpose, we use the trapezium rule as an LMS method. It is an A -stable rule and hence condition (3.10a) is fulfilled for all h . Hence, if $\Sigma_{ch}(\mathbb{C}^+) \subseteq \Sigma_c(\mathbb{C}^+)$ (equivalently, $\Sigma_h(\tau_1, \tau_2; \mathbb{C}^+) \subseteq \Sigma(\tau_1, \tau_2; \mathbb{C}^+)$) then RHP-stability is recovered by the discretized equation. We choose A_0 , A_1 , τ_1 and τ_2 in (1.2) such that $\Sigma_c(\mathbb{C}^+) \subset \mathbb{C}_0^-$, cf. fig. 7, and hence the zero solution of (1.2) is stable. The use of Simpson’s rule with $h = \tau_1$ for the example shown in this figure gives a false unstable root, $\lambda \simeq 0.396 \pm 49.737i$, although the outside part of the region $\Sigma_{ch}(\mathbb{C}^+)$ w.r.t. $\Sigma_c(\mathbb{C}^+)$ is relatively small. Decreasing h , the boundary of Σ_{ch} approaches the boundary of Σ_c and the numerical solution becomes stable. Note that the use of the proposed quadrature scheme gives stable roots for any $h = \tau_1/n$, $n = 1, 2, \dots$

In our tests on the convergence orders for the characteristic root approximations, we use the implicit backward differentiation (BDF) method with different number of steps, $k = 3, 4, 5, 6$, and m -point Gauss-Legendre quadrature rule with $m = s_- + 1$, $s_- = 1, 2$, i.e. the quadrature has degree of precision, $q := 2m - 1 = 2s_- + 1 = s_- + s_+$, equal to the degree of the Lagrange polynomial that we use (always assuming $s_+ = s_- + 1$).

The rightmost roots of the characteristic equation (3.4) for $A_0 = -4$, $A_1 = -3$, $\tau_2 = 4$ are depicted in fig. 8 (left) for $\tau_1 = 1$ and $\tau_1 = 0$. For $\tau_1 = 1$, the convergence towards the

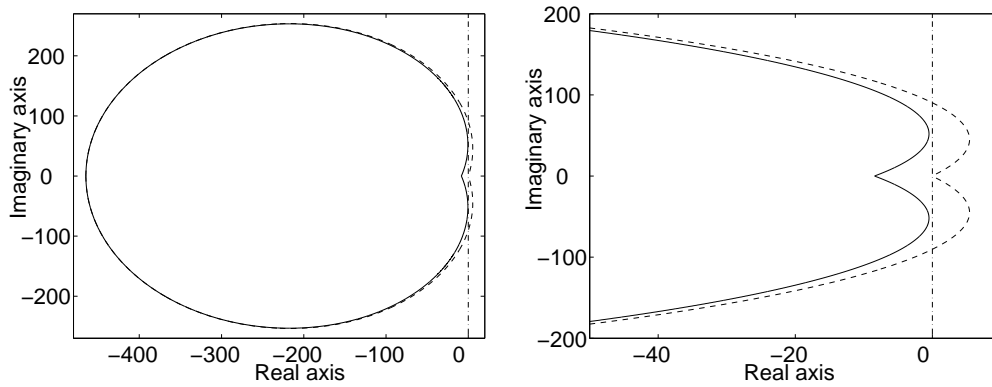


Figure 7: Left: Regions $\Sigma_c(\mathbb{C}^+)$ and $\Sigma_{ch}(\mathbb{C}^+)$ are bounded by a solid respectively dashed line. $A_0 = -186$, $A_1 = -4905$, $\tau_1 = 0.0285$ and $\tau_2 = 0.0855$. Σ_{ch} corresponds to Simpson's rule. Right: a blow up of the left figure.

rightmost root $\lambda_1 \simeq 0.069 - 1.176i$ (computed with accuracy 10^{-13} using a Newton iteration on the characteristic equation) by the corresponding root, λ_1^h , of the characteristic equation (3.5) is shown in fig. 8 (right) for varying h , $h = 1/L$, $L = 10, \dots, 100$, and various BDF methods. Table 1 gives the numerical approximation of the convergence order based on a least squares approximation of the results for $L = 10, \dots, 100$ using BDF methods with $k = 3, 4, 5, 6$ steps and Gauss-Legendre quadrature rule with degree of precision $q = 3, 5$. The $\mathcal{O}(h^{\min(k, q+1)})$ convergence is clearly apparent. This is in agreement with proven results on the convergence order for solutions of numerical schemes for DIDEs obtained by applying an LMS method combined with a quadrature rule [4]. For the case $\tau_1 = 0$ we have obtained similar results. The rates of convergence of all roots are similar but have different error constants.

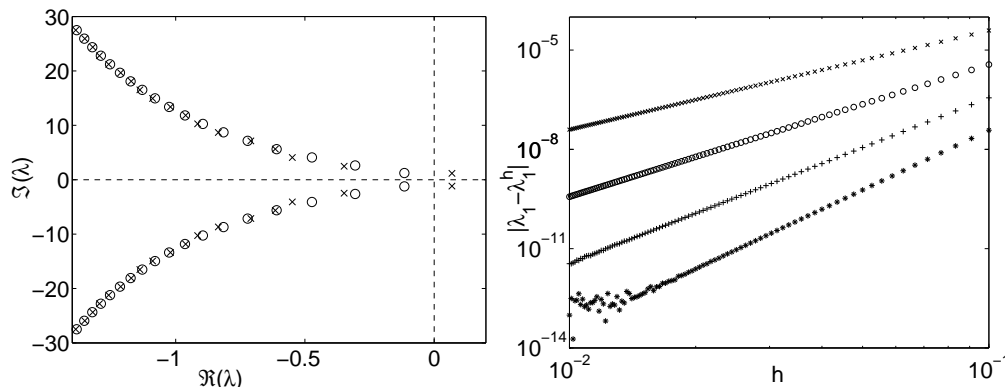


Figure 8: Left: The rightmost roots of the characteristic equation (3.4) for $\tau_1 = 1$ (x), $\tau_1 = 0$ (o). Right: Convergence of the rightmost characteristic root of (3.5), λ_1^h , to the root λ_1 in the case $\tau_1 = 1$ for varying $h = 1/L$, $L = 10, \dots, 100$, and different number of steps k of BDF methods, $k = 3$ (x), $k = 4$ (o), $k = 5$ (+) and $k = 6$ (*). $A_0 = -4$, $A_1 = -3$, $\tau_2 = 4$. Here Gauss-Legendre quadrature was used with $m = 3$ (i.e. $s_- = 2$).

It is interesting to note that formula (3.11) for the steplength h applied to the example illustrated in fig. 8 with $\tau_1 = 0$ gives, e.g. $h \simeq 0.036$ using the 4-step BDF method. We

	$k = 3$	$k = 4$	$k = 5$	$k = 6$
$m = 2$	2.990	3.978	4.083	4.005
$m = 3$	2.997	3.996	5.007	5.997

Table 1: Numerically observed orders of convergence while approximating the rightmost root λ_1 of (3.4) with $A_0 = -4$, $A_1 = -3$, $\tau_1 = 1$, $\tau_2 = 4$, using BDF methods with $k = 3, 4, 5, 6$ steps and Gauss-Legendre quadratures with $m = 2, 3$ (i.e. $s_- = 1, 2$).

know (cf. section 4) that $\Sigma_{h,GL}(0, \tau_2; \mathbb{C}^+) \not\subseteq \Sigma(0, \tau_2; \mathbb{C}^+)$ when the proposed quadrature scheme is used with $s_- \geq 1$ in the Lagrange interpolation. Fig. 9 illustrates a significant difference in the size of the outside part of the regions $\Sigma_{h,GL}(0, \tau_2; \mathbb{C}^+)$ and $\Sigma_{h,NC}(0, \tau_2; \mathbb{C}^+)$ compared to the region $\Sigma(0, \tau_2; \mathbb{C}^+)$ when using the proposed quadrature and Simpson's rule with $h = 0.1/3$. In both cases, the boundary of $\Sigma_{h,GL}$ and $\Sigma_{h,NC}$ approximates well the boundary of Σ (located slightly outside Σ) except for the parts depicted in grey. Despite this difference, the use of Simpson's rule leads to a correct approximation of the rightmost characteristic roots.

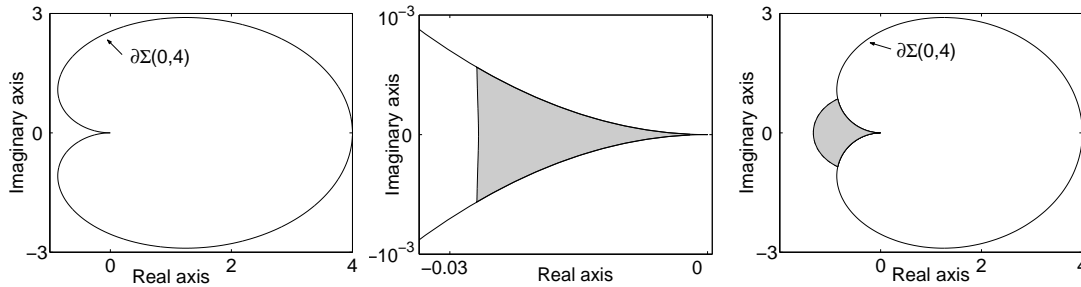


Figure 9: The outside part of $\Sigma_{h,GL}(0, \tau_2; \mathbb{C}^+)$ and $\Sigma_{h,NC}(0, \tau_2; \mathbb{C}^+)$ w.r.t. $\Sigma(0, \tau_2; \mathbb{C}^+)$ is depicted in grey. Left: Gauss-Legendre quadrature rule with $m = 2$ (i.e. $s_- = 1$). Middle: a blow up of the left figure. Right: Simpson's rule. $\tau_2 = 4$, $h = 0.1/3$.

5.2 Non-constant kernel function

Our analysis of the proposed quadrature applied to the integral of (1.2) with a constant kernel function gives insight into the properties of the quadrature when using a non-constant kernel. In particular, the analysis suggests to distinguish two cases: $\tau_1 \neq 0$ and $\tau_1 = 0$. Note that results similar to theorems 3.1, 3.2 and 3.3 can be proven for the considered (bounded and analytic) kernel functions. So, in our numerical experiments we are also interested whether condition (3.12) is fulfilled by the proposed quadrature.

- Case $\tau_1 \neq 0$.

In this case, all our tests with non-constant kernel functions (combinations of trigonometric and polynomial functions) showed that $\Sigma_{h,GL}(\tau_1, \tau_2; \mathbb{C}^+) \subseteq \Sigma(\tau_1, \tau_2; \mathbb{C}^+)$. However there is no guarantee that this property holds in general. Nevertheless, we expect that when the property is violated, the approximation of the boundary of $\Sigma(\tau_1, \tau_2; \mathbb{C}^+)$ by the boundary of $\Sigma_{h,GL}(\tau_1, \tau_2; \mathbb{C}^+)$ should be good enough to allow a correct approximation of the rightmost characteristic roots.

As an illustrative example, we use the kernel function $K(\xi) = (5 - \xi) \cos(6\xi) + 2.5$, $\xi \in [2, 5]$. We computed the rightmost roots of the characteristic equation (3.1), see fig. 10 (left). Results on the convergence orders for the characteristic root approximations are similar to the ones obtained in case of a constant kernel function, cf. tables 2 and 1.

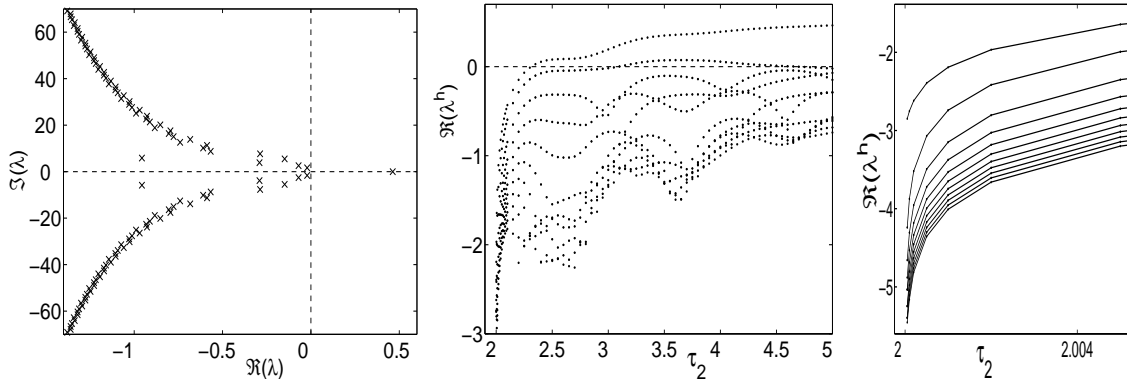


Figure 10: Left: The rightmost roots of the characteristic equation (3.1) for $\tau_1 = 2$, $\tau_2 = 5$. Middle: Evolution of 20 rightmost roots λ^h as $\tau_2 \rightarrow \tau_1$. Right: A blow up of the middle figure. For clarity, evolution of the same root is depicted by a solid line. The 6-step BDF method and 3-point Gauss-Legendre quadrature rule were used. $A_0 = -3$, $A_1 = 2$, $K(\xi) = (5 - \xi) \cos(6\xi) + 2.5$, $\xi \in [2, 5]$.

	$k = 3$	$k = 4$	$k = 5$	$k = 6$
$m = 2$	3.010	4.024	3.825	3.979
$m = 3$	3.000	4.000	5.002	6.004

Table 2: Numerically observed orders of convergence while approximating the second rightmost root ($\lambda_2 \simeq -0.021 - 1.649i$) of (3.1) with $A_0 = -3$, $A_1 = 2$, $\tau_1 = 2$, $\tau_2 = 5$, $K(\xi) = (5 - \xi) \cos(6\xi) + 2.5$, $\xi \in [2, 5]$, using BDF methods with $k = 3, 4, 5, 6$ steps and Gauss-Legendre quadratures with $m = 2, 3$ (i.e. $s_- = 1, 2$).

Using the same kernel function, we performed the following experiment. Equation (1.2) is an ordinary differential equation with a single characteristic root $\lambda = -A_0$ when $\tau_1 = \tau_2$. The evolution of the 21 rightmost roots λ^h (one real and others complex-conjugated) as $\tau_2 \rightarrow \tau_1$ is depicted in fig. 10 (middle, right) for the example shown in the left figure. These computations were done for a number of values of τ_2 approaching τ_1 . We observe that as $\tau_2 \rightarrow \tau_1$, the stability of the zero solution changes, $\lambda_1^h \rightarrow -3$ ($\lambda_1^h \simeq -2.85$ at $\tau_2 = 2.00005$) and all other roots rapidly decrease.

- Case $\tau_1 = 0$.

Our experiments with $\tau_1 = 0$ have suggested to distinguish between two types of kernel functions: in a neighborhood of $\xi = 0$, as $\xi \rightarrow 0$, (a) $K(\xi)$ is a decreasing function and (b) $K(\xi)$ is not a decreasing function. In applications these types of $K(\xi)$ can correspond to situations when: (a) the effect of a certain moment in the past, e.g. at time $t - \tau$, is smoothed over a finite interval $[t - \tau_2, t]$ such that $K(\xi)$ peaks at $\xi = \tau$, $0 < \tau < \tau_2$, and is small elsewhere, and (b) an infinite distributed delay is approximated by a finite one, cutting a decaying (as $\xi \rightarrow \infty$) kernel function.

Some results of numerical experiments corresponding to the first case are given in table 3 for $K(\xi) = \sin(\xi) + \alpha$. Numerically obtained estimates of h (satisfying $h = \tau_2/n$, $n = 1, 2, \dots$) presented in this table, guarantee that $\Sigma_{h, GL}(0, \tau_2; \mathbb{C}^+) \subset \Sigma(0, \tau_2; \mathbb{C}^+)$. It follows that the higher accuracy of the quadrature rule, the smaller h has to be to preserve this property. Also, the behaviour of $K(\xi)$ far away from the point $\xi = 0$ influences the properties of the numerical schemes (cf. results for $\tau_2 = 1.5$ and $\tau_2 = 3$).

	$\tau_2 = 1.5$			$\tau_2 = 3$		
	$\alpha = 0$	$\alpha = 1$	$\alpha = 5$	$\alpha = 0$	$\alpha = 1$	$\alpha = 5$
$s_- = 0$	$h \leq \tau_2$	$h \leq \tau_2$	$h \leq \tau_2$	$h \leq \tau_2$	$h \leq \tau_2$	$h \leq \tau_2$
$s_- = 1$	$h \leq \frac{\tau_2}{2}$	$h \leq \frac{\tau_2}{3}$	$h \leq \frac{\tau_2}{6}$	$h \leq \frac{\tau_2}{3}$	$h \leq \frac{\tau_2}{4}$	$h \leq \frac{\tau_2}{10}$
$s_- = 2$	$h \leq \frac{\tau_2}{2}$	$h \leq \frac{\tau_2}{4}$	$h \leq \frac{\tau_2}{10}$	$h \leq \frac{\tau_2}{3}$	$h \leq \frac{\tau_2}{5}$	$h \leq \frac{\tau_2}{18}$

Table 3: Numerically obtained estimates for the step size h ($h = \tau_2/n$, $n = 1, 2, \dots$) which guarantee that $\Sigma_{h, GL}(0, \tau_2; \mathbb{C}^+) \subset \Sigma(0, \tau_2; \mathbb{C}^+)$. Here $K(\xi) = \sin(\xi) + \alpha$, $\xi \in [0, \tau_2]$.

In the second case, all our experiments have shown that $\Sigma_{h, GL}(0, \tau_2; \mathbb{C}^+) \not\subset \Sigma(0, \tau_2; \mathbb{C}^+)$ for any h . This case includes a constant kernel function. Hence, results shown in fig. 4 are rather illustrative for non-constant kernels of this type: the boundary of $\Sigma_{h, GL}$ approaches the boundary of Σ as $h \rightarrow 0$.

Note that in the case $\tau_1 = 0$, results on the convergence orders for the characteristic root approximations are similar to the ones presented in tables 1 and 2.

6 Conclusion

Numerical stability analysis of delay integro-differential equations (DIDEs) is still an open area. In practical computations, one should use numerical schemes that retain the stability properties of the original equation. The analysis presented in this paper addresses this problem for scalar DIDEs and commensurate delays.

We have proposed a quadrature method based on Lagrange interpolation and a Gauss-Legendre quadrature rule in combination with a linear multistep (LMS) method for time integration. Aiming at the analysis of stability properties of the proposed scheme, we derived and proved a sufficient condition for the stability of a DIDE with a constant kernel which we term RHP-stability. We obtained conditions under which the stability is preserved by the proposed scheme. When these conditions are not fulfilled, we showed that the proposed scheme remains preferable to Newton-Cotes formulas which do not retain RHP-stability.

Using the proposed scheme, we present results on the convergence orders of numerical approximations to the rightmost (stability determining) roots of the characteristic equation associated with the original equation. These results are in agreement with proven results on the convergence order for solutions of numerical schemes for DIDEs obtained by applying an LMS method combined with a quadrature rule [4].

One of the most important issues in the stability analysis of DIDEs is the effect of the kernel function on the stability of the applied numerical scheme. Our analytical results

for a constant kernel and numerical experiments for non-constant kernels suggest that the proposed scheme can retain RHP-stability of the original equation with a rather general kernel if the effect of the past is distributed over the interval $[t - \tau_2, t - \tau_1]$ with $\tau_2 > \tau_1 > 0$, i.e. $\tau_1 \neq 0$.

Future research can be directed towards systems of DIDEs with non-commensurate delays and when the delay τ_1 equals or approaches zero.

Acknowledgments

This research presents results of the Research Project OT 98/16, funded by the Research Council K.U.Leuven, of the Project G.0270.00 funded by the Fund for Scientific Research - Flanders (Belgium) and of the Project IUAP P5/22 funded by the programme on Inter-university Poles of Attraction, initiated by the Belgian State, Prime Minister's Office for Science, Technology and Culture. K. Engelborghs is a Postdoctoral Fellow of the Fund for Scientific Research - Flanders (Belgium).

A Appendix. Proofs of theorems

A.1 Necessary results

To prove theorems 3.1, 3.2 and 3.3, we need the following lemma.

Lemma A.1 *If $f(z)$ is analytic and $\lim_{|z| \rightarrow \infty} f(z) = z_\infty \in \mathbb{C}$ uniformly then $\bigcup_{\Re(z) \geq 0} f(z)$ is inside the curve $\bigcup_{\theta \in \mathbb{R}} f(i\theta)$.*

Proof. Let $M > 0$ be such that $|f(i\theta)| < M$, $\forall \theta \in \mathbb{R}$. Let a point $q \in \mathbb{C}$ be outside the region bounded by $\bigcup_{\theta \in \mathbb{R}} f(i\theta)$. Then there exists a curve C_0 starting at q and ending at a point b with $|b| > M$ which does not intersect $\bigcup_{\theta \in \mathbb{R}} f(i\theta)$.

Consider the contour C_R which consists of the imaginary axis up to $\{i\theta \mid |\theta| \leq R\}$ and the semicircle $\{z \mid \Re(z) \geq 0, |z| = R\}$. Let r_0 denote the smallest distance of the curve C_0 to the point z_∞ . We choose R big enough such that $|f(z) - z_\infty| < r_0$ for $|z| \geq R$. Let closed contours J_R and Q_R define the images of the contour C_R under the mappings $J = f(z)$ respectively $Q = f_q(z)$, $f_q(z) := f(z) - q$. It follows from the above that the curve C_0 and the contour J_R (equivalently, curves $C_0 - q$ and Q_R) do not intersect. As a consequence, q lies outside J_R , and, equivalently, the origin lies outside Q_R .

This implies that the curve Q_R does not encircle the origin, and, due to the argument principle applied to $f_q(z)$ and contour C_R , the number of zeros of $f_q(z)$ equals the number of poles of $f_q(z)$ in the interior of C_R . Since $f_q(z)$ has no poles, it can have no zeros and hence $f(z) \neq q$ within C_R . As the latter holds for R arbitrarily large, it is clear that $f(z) \neq q$ for all z , $\Re(z) \geq 0$ which proves the lemma. \square

To prove theorem 4.1, we need certain properties of coefficients ω_l of the quadrature (2.5),

$$\omega_l = \sum_{k=1}^m B_k P_l(\epsilon_k), \quad l = -s_-, \dots, s_+. \quad (\text{A.1.1})$$

Recall that $\epsilon_k h$ and B_k are the zeros of the m th-degree Legendre polynomial respectively weights of the Gauss-Legendre quadrature on $[0, h]$ and $P_l(\epsilon_k)$ are the Lagrange coefficients,

$$P_l(\epsilon_k) = \prod_{\nu=-s_-, \nu \neq l}^{s_+} \frac{\epsilon_k - \nu}{l - \nu}, \quad \epsilon_k \in [0, 1], \quad l = -s_-, \dots, s_+. \quad (\text{A.1.2})$$

Let $v(\epsilon) := (\epsilon + s_-)(\epsilon + s_- - 1) \cdots (\epsilon + 1)\epsilon(\epsilon - 1) \cdots (\epsilon - s_+)$ and $v'(j) = (dv(\epsilon)/d\epsilon)_{\epsilon=j}$. Then (A.1.2) reads

$$P_l(\epsilon_k) = \frac{v(\epsilon_k)}{(\epsilon_k - l)v'(l)}. \quad (\text{A.1.3})$$

Assume that $s_+ = s_- + 1$. Points ϵ_k and ϵ_{m-k+1} , $k = 1, \dots, \lfloor \frac{m}{2} \rfloor$ ($\lfloor r \rfloor$ denotes the smallest integer less than or equal to $r \in \mathbb{R}$), are symmetric with respect to $1/2$, i.e. $\epsilon_k = 1 - \epsilon_{m-k+1}$. Note also that $v(\epsilon_k) = v(1 - \epsilon_k)$ and $v'(l) = -v'(1 - l)$, $l = -s_-, \dots, 0$. Hence, using (A.1.3), we obtain

$$P_l(\epsilon_k) = P_{1-l}(1 - \epsilon_k), \quad P_l(0.5) = P_{1-l}(0.5), \quad k = 1, \dots, \lfloor \frac{m}{2} \rfloor, \quad l = -s_-, \dots, 0. \quad (\text{A.1.4})$$

Using (A.1.4) and that $B_k = B_{m-k+1}$, $k = 1, \dots, \lfloor \frac{m}{2} \rfloor$, [19], we obtain

$$\begin{aligned} \omega_l &= \sum_{k=1}^m B_k P_l(\epsilon_k) = \sum_{k=1}^m B_k P_{1-l}(1 - \epsilon_k) = \sum_{k=1}^m B_k P_{1-l}(1 - \epsilon_{m-k+1}) \\ &= \sum_{k=1}^m B_k P_{1-l}(\epsilon_k) = \omega_{1-l}, \quad l = -s_-, \dots, 0. \end{aligned} \quad (\text{A.1.5})$$

A.2 Proof of theorem 3.1

Let $F(\lambda) := \int_{\tau_1}^{\tau_2} e^{-\lambda\xi} d\xi$. $F(\lambda)$ is analytic and $F(\lambda) \rightarrow 0$ uniformly as $|\lambda| \rightarrow \infty$. Hence, due to lemma A.1, $\bigcup_{\Re(\lambda) \geq 0} F(\lambda)$ is inside the curve $\bigcup_{\theta \in \mathbb{R}} F(i\theta)$. \square

A.3 Proof of theorem 3.2

Let $F(\lambda) := \sum_{r=1}^{n_c} \sum_{l=-s_-}^{s_+} \omega_l e^{-\lambda h(q_{1,r}-l)} + \sum_{r=1}^{n_s} \sum_{l=-s(r)_-}^{s(r)_+} \omega_{l,r} e^{-\lambda h(q_{2,r}-l)}$.

If $\tau_1 \geq (s_+ - 1)h$, then $n_c = n$ and $n_s = 0$. Hence

$$F(\lambda) = \sum_{r=1}^n \sum_{l=-s_-}^{s_+} \omega_l e^{-\lambda h(n_2-r+1-l)}$$

and $\lim_{|\lambda| \rightarrow \infty} F(\lambda) = \omega_{s_+}$ uniformly if $\tau_1 = (s_+ - 1)h$, and $\lim_{|\lambda| \rightarrow \infty} F(\lambda) = 0$ uniformly otherwise.

If $\tau_1 < (s_+ - 1)h$, then $n_c = n_2 - s_+ + 1$ and $n_s = s_+ - 1 - n_1$. Hence

$$F(\lambda) = \sum_{r=1}^{n_2-s_++1} \sum_{l=-s_-}^{s_+} \omega_l e^{-\lambda h(n_2-r+1-l)} + \sum_{r=1}^{s_+-1-n_1} \sum_{l=-s(r)_-}^{s(r)_+} \omega_{l,r} e^{-\lambda h(s_+-r-l)}$$

and $\lim_{|\lambda| \rightarrow \infty} F(\lambda) = \sum_{r=1}^{s_+-1-n_1} \omega_{s(r)_+,r}$ uniformly if $\tau_2 = (s_+ - 1)h$, and $\lim_{|\lambda| \rightarrow \infty} F(\lambda) = \omega_{s_+} + \sum_{r=1}^{s_+-1-n_1} \omega_{s(r)_+,r}$ uniformly otherwise.

Due to lemma A.1, $\bigcup_{\Re(\lambda) \geq 0} F(\lambda)$ is inside the curve $\bigcup_{\theta \in \mathbb{R}} F(i\theta)$. \square

A.4 Proof of theorem 3.3

Let $F(\lambda) := \sum_{r=1}^{n_m} \sum_{l=1}^m \omega_l e^{-\lambda h(q_r - l + 1)} = e^{-\lambda \tau_1} \sum_{r=1}^{n_m} e^{-\lambda h(r-1)(m-1)} \sum_{l=1}^m \omega_l e^{\lambda h(l-m)}$. If $\tau_1 = 0$, then $\lim_{|\lambda| \rightarrow \infty} F(\lambda) = \omega_m$ uniformly and $\lim_{|\lambda| \rightarrow \infty} F(\lambda) = 0$ uniformly otherwise. Hence, due to lemma A.1, $\bigcup_{\Re(\lambda) \geq 0} F(\lambda)$ is inside the curve $\bigcup_{\theta \in \mathbb{R}} F(i\theta)$. \square

A.5 Proof of lemma 4.1

Let

$$S(\theta) := \int_0^h e^{-i\theta \xi} d\xi = \frac{\sin(\theta h) + i(\cos(\theta h) - 1)}{\theta}, \quad S_h(\theta) := \sum_{l=-s_-}^{s_+} \omega_l e^{i\theta h(l-1)}.$$

Obviously,

$$\Sigma(0, h; \bigcup_{\theta \in \mathbb{R}} i\theta) \equiv \bigcup_{\theta \in \mathbb{R}} S(\theta), \quad \partial \Sigma(0, h) \equiv \bigcup_{\theta \in [-\frac{2\pi}{h}, \frac{2\pi}{h}]} S(\theta)$$

and

$$\Sigma_{h, GL}(0, h; \bigcup_{\theta \in \mathbb{R}} i\theta) \equiv \bigcup_{\theta \in \mathbb{R}} S_h(\theta), \quad \partial \Sigma_{h, GL}(0, h) \equiv \bigcup_{\theta \in [-\frac{\pi}{h}, \frac{\pi}{h}]} S_h(\theta).$$

Let

$$S_0(\theta) := S(\theta), \quad \theta \in [-\frac{2\pi}{h}, \frac{2\pi}{h}], \\ S_j^+(\theta) := S(\theta), \quad \theta \in [\frac{2\pi j}{h}, \frac{2\pi(j+1)}{h}], \quad S_j^-(\theta) := S(\theta), \quad \theta \in [-\frac{2\pi j}{h}, -\frac{2\pi(j+1)}{h}], \quad j = 1, 2, \dots$$

Hence the curve $\bigcup_{\theta \in \mathbb{R}} S(\theta)$ can be considered as an union of branches $S_0(\theta)$ and $S_j^\pm(\theta)$, $j = 1, 2, \dots$. All these branches are closed curves since $S(\theta)$ is symmetric w.r.t. the real axis and $\Im(S(0)) = \Im(S(\pm 2\pi j/h)) = \Re(S(\pm 2\pi j/h)) = 0$, $j = 1, 2, \dots$. Considering $S(\theta)$ as a $2\pi/h$ periodic function in θ divided by θ , it follows that $|S_j^+| \leq |S_0|$, $\arg(S_j^+(\theta)) = \arg(S_0(\theta))$, $\tilde{\theta} \in [2\pi j/h, 2\pi(j+1)/h]$, $\theta \in [0, 2\pi/h]$, and similar for S_j^- , $j = 1, 2, \dots$. Therefore S_j^\pm , $j = 1, 2, \dots$, are located inside S_0 and hence inside $\partial \Sigma$.

The second part of the lemma is due to: $S_h(\theta)$ is $2\pi/h$ periodic, symmetric w.r.t. the real axis and $\Im(S_h(0)) = \Im(S_h(\pm\pi/h)) = 0$. \square

A.6 Proof of theorem 4.1 and corollary 4.1

A.6.1 Proof of theorem 4.1

Let

$$S(\theta) := \int_0^h e^{-i\theta \xi} d\xi = h \int_0^1 e^{i\theta h(\epsilon-1)} d\epsilon = \frac{\sin(\theta h) + i(\cos(\theta h) - 1)}{\theta}, \quad \epsilon \in [0, 1],$$

$$S_h(\theta) := h \int_0^1 P(i\theta h, \epsilon) d\epsilon = \sum_{l=-s_-}^{s_+} \omega_l e^{i\theta h(l-1)}, \quad P(i\theta h, \epsilon) := \sum_{l=-s_-}^{s_+} P_l(\epsilon) e^{i\theta h(l-1)}. \quad (\text{A.6.1})$$

Due to lemma 4.1, $\partial \Sigma$ and $\partial \Sigma_{h, GL}$ are closed curves, $\partial \Sigma = S(\theta)$, $\theta \in [-2\pi/h, 2\pi/h]$ and $\partial \Sigma_{h, GL} = S_h(\theta)$, $\theta \in [-\pi/h, \pi/h]$.

The statement of the theorem, $\partial \Sigma_{h, GL}$ is inside $\partial \Sigma$, follows from the following results which we will prove successively below,

- 1) if $s_+ = s_- + 1$, then $\arg(S_h(\theta)) = \arg(S(\theta))$, $\theta \in [-\pi/h, \pi/h]$;
- 2) if $s_+ = s_- + 1$, then $|S_h(\theta)| \leq |S(\theta)|$, $\theta \in [-\pi/h, \pi/h]$.

Step 1. Using the assumption $s_+ = s_- + 1$ and (A.1.5), we obtain

$$\begin{aligned} S_h(\theta) &= \sum_{l=-s_-}^0 \omega_l (e^{i\theta h(l-1)} + e^{i\theta h(-l)}) = e^{-i\frac{\theta h}{2}} \sum_{l=-s_-}^0 \omega_l (e^{i\theta h(l-\frac{1}{2})} + e^{-i\theta h(l-\frac{1}{2})}) \\ &= e^{-i\frac{\theta h}{2}} \sum_{l=-s_-}^0 2\omega_l \cos(\theta h(l - \frac{1}{2})) = e^{-i\frac{\theta h}{2}} Q, \quad Q \in \mathbb{R}, \quad \theta \in [-\frac{\pi}{h}, \frac{\pi}{h}]. \end{aligned} \quad (\text{A.6.2})$$

Hence $\arg(S_h(\theta)) = -\theta h/2$. It follows from (A.6.1) that

$$\arg(S(\theta)) = \tan^{-1} \left(\frac{\cos(\theta h) - 1}{\sin(\theta h)} \right) = \tan^{-1} \left(\frac{-\sin(\theta h/2)}{\cos(\theta h/2)} \right) = -\frac{\theta h}{2}, \quad \theta \in [-\frac{\pi}{h}, \frac{\pi}{h}].$$

Step 2. Consider functions $P(i\theta h, \epsilon)$ and $e^{i\theta h(\epsilon-1)}$, i.e. integrands in the definition of $S_h(\theta)$ and $S(\theta)$, cf. (A.6.1). Let $z := e^{i\theta h}$. Then $P(i\theta h, \epsilon)$ can be considered as a polynomial in z . Since $|z| = 1$, $s_+ = s_- + 1$ and $|e^{i\theta h(\epsilon-1)}| = 1$, it follows [18, 13] for any $\epsilon \in [0, 1]$ that

$$|P(i\theta h, \epsilon)| = \left| z^{-s_- - 1} \sum_{l=-s_-}^{s_+} P_l(\epsilon) z^{l+s_-} \right| \leq 1, \quad \text{and hence } |P(i\theta h, \epsilon)| \leq |e^{i\theta h(\epsilon-1)}|. \quad (\text{A.6.3})$$

Now consider $P(i\theta h, \epsilon)$ and $e^{i\theta h(\epsilon-1)}$ as functions in ϵ (cf. fig. 11). For any $\theta \in (0, \pi/h)$ we have:

- (i) $P(i\theta h, \epsilon)|_{\epsilon=0} = e^{i\theta h(\epsilon-1)}|_{\epsilon=0} = e^{-i\theta h}$, $P(i\theta h, \epsilon)|_{\epsilon=1} = e^{i\theta h(\epsilon-1)}|_{\epsilon=1} = 1$.
- (ii) $\Im(e^{i\theta h(\epsilon-1)}) < 0$ and $\Im(P(i\theta h, \epsilon)) < 0$, $\epsilon \in (0, 1)$.

The latter follows from the following. For $s_- = 0$ we have $P(i\theta h, \epsilon) = P_0(\epsilon)e^{-i\theta h} + P_1(\epsilon) = (1 - \epsilon)e^{-i\theta h} + \epsilon$ and hence $\Im(P(i\theta h, \epsilon)) < 0$. For a fixed s_- , let Q_1 and Q_2 denote $P_0(\epsilon)$ associated with $s_- - 1$ and s_- , respectively. Then $Q_2/Q_1 = (\epsilon + s_-)(s_+ - \epsilon)/(s_- s_+) \simeq 1$. Hence $P_0(\epsilon)$ does not depend on s_- significantly and similar holds for P_l , $l = -s_-, \dots, s_+$. Since $\sum_{l=-s_-}^{s_+} P_l(\epsilon) = 1$, it follows that coefficients $P_0(\epsilon)$ and $P_1(\epsilon)$ are dominant ones. As a result, $\Im(P(i\theta h, \epsilon)) < 0$, $\forall s_-$.

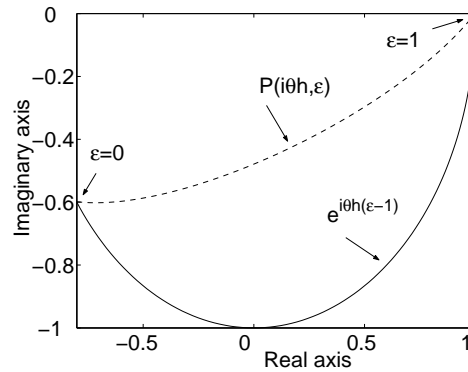


Figure 11: In the complex plane, $P(i\theta h, \epsilon)$ (dashed curve) and $e^{i\theta h(\epsilon-1)}$ (solid curve) as functions in ϵ , $\epsilon \in [0, 1]$. $h = 1$, $\theta = 2.5$, $s_- = 1$, $s_+ = 2$.

Note that property (ii) implies that $P(i\theta h, \epsilon)$ does not cross the real axis whenever $\epsilon \in (0, 1)$ and $\theta \in (0, \pi/h)$. Due to (A.6.3), (i) and (ii), we conclude that $|S_h(\theta)| < |S(\theta)|$ for $\theta \in (0, \pi/h)$. Taking into account that $|S_h(0)| = |S(0)| = h$, $|S_h(\pi/h)| = 0$ and $|S(\pi/h)| = 2h/\pi$, it follows that $|S_h(\theta)| \leq |S(\theta)|$, $\theta \in [0, \pi/h]$.

Due to the symmetry of $S_h(\theta)$ and $S(\theta)$ w.r.t. the real axis, $|S_h(\theta)| < |S(\theta)|$, $\theta \in [-\pi/h, 0)$. \square

A.6.2 Proof of corollary 4.1

The corollary is due to

$$\begin{aligned} \Sigma(\tau_1, \tau_2; \bigcup_{\theta \in \mathbb{R}} i\theta) &= \bigcup_{\theta \in \mathbb{R}} \left(\int_{\tau_1}^{\tau_2} e^{-i\theta\xi} d\xi \right) = \bigcup_{\theta \in \mathbb{R}} \left(e^{-i\theta\tau_1} \sum_{r=1}^n e^{-i\theta(r-1)h} \int_0^h e^{-i\theta\xi} d\xi \right) \\ &= \bigcup_{\theta \in \mathbb{R}} \left(Q(\theta) \int_0^h e^{-i\theta\xi} d\xi \right), \quad Q(\theta) := e^{-i\theta\tau_1} \sum_{r=1}^n e^{-i\theta(r-1)h} \in \mathbb{C}, \\ \Sigma_{h, GL}(\tau_1, \tau_2; \bigcup_{\theta \in \mathbb{R}} i\theta) &= \bigcup_{\theta \in \mathbb{R}} \left(e^{-i\theta\tau_1} \sum_{r=1}^n e^{-i\theta(r-1)h} \sum_{l=-s_-}^{s_+} \omega_l e^{i\theta h(l-1)} \right) \\ &= \bigcup_{\theta \in \mathbb{R}} \left(Q(\theta) \sum_{l=-s_-}^{s_+} \omega_l e^{i\theta h(l-1)} \right), \end{aligned}$$

and theorem 4.1. \square

References

- [1] O. Arino, M. L. Hbid, and R. B. de la Parra. A mathematical model of growth of population of fish in the larval stage: Density-dependence effects. *Math. Biosc.*, 150:1–20, 1998.
- [2] C. T. H. Baker and N. J. Ford. Some applications of the boundary-locus method and the method of D-partitions. *IMA J. Num. Analysis*, 11:143–158, 1991.
- [3] C. T. H. Baker and N. J. Ford. Stability properties of a scheme for the approximate solution of a delay-integro-differential equation. *Appl. Numer. Math.*, 9:357–370, 1992.
- [4] C. T. H. Baker and N. J. Ford. Asymptotic error expansions for linear multistep methods for a class of delay integro-differential equations. In Lipitakis E. A, editor, *Advances on Computer Mathematics and its Applications*, pages 59–72. World Scientific, 1993.
- [5] K. Engelborghs, T. Luzyanina, and D. Roose. Numerical bifurcation analysis of delay differential equations using DDE-BIFTOOL. *ACM Trans. Math. Softw.*, 28(1), 2002. To appear.
- [6] K. Engelborghs, T. Luzyanina, and G. Samaey. DDE-BIFTOOL v. 2.00: a Matlab package for bifurcation analysis of delay differential equations. Technical Report TW-330, Department of Computer Science, K.U.Leuven, Leuven, Belgium, 2001. Available from <http://www.cs.kuleuven.ac.be/~koen/delay/ddebiftool.shtml>.
- [7] K. Engelborghs and D. Roose. On stability of LMS-methods and characteristic roots of delay differential equations. *SIAM J. Num. Analysis*, 2001. Accepted.

- [8] E. Hairer, S. P. Norsett, and G. Wanner. *Solving ordinary differential equations. 1: Nonstiff problems*, volume 8 of *Springer series in computational mathematics*. Springer Berlin, 2nd edition, 1993.
- [9] J. K. Hale and S. M. Verduyn Lunel. *Introduction to Functional Differential Equations*, volume 99 of *Applied Mathematical Sciences*. Springer-Verlag, 1993.
- [10] H. W. Hethcote, M. A. Lewis, and P. van den Driessche. An epidemiological model with a delay and a nonlinear incidence rate. *J. Math. Biol.*, 27:49–64, 1989.
- [11] T. Hong-Jiong and K. Jiao-Xun. The numerical stability of linear multistep methods for delay differential equations with many delays. *SIAM J. Numer. Anal.*, 33(3):883–889, 1996.
- [12] E. Isaacson and H. B. Keller. *Analysis of numerical methods*. J. Wiley & Sons, Inc., New York, 1966.
- [13] A. Iserles and G. Strang. The optimal accuracy of difference schemes. *Trans. Amer. Math. Soc.*, 277:779–803, 1983.
- [14] V. Kolmanovskii and A. Myshkis. *Introduction to the Theory and Applications of Functional Differential Equations*, volume 463 of *Mathematics and its Applications*. Kluwer Academic Publishers, Dordrecht, 1999.
- [15] T. Koto. Stability of Runge-Kutta methods for delay integro-differential equations. *J. Comput. and Appl. Math.*, 2001. Accepted.
- [16] Y. Kuang. *Delay Differential Equations with Applications in Population Dynamics*. Academic Press, San Diego, 1993.
- [17] Y. Li and Y. Kuang. Periodic solutions of periodic delay Lotka-Volterra equations and systems. *J. Math. Anal. Appl.*, 255:260–280, 2001.
- [18] G. Strang. Trigonometric polynomials and difference methods of maximum accuracy. *J. Math. and Phys.*, 41:147–154, 1962.
- [19] A. H. Stroud and D. Secrest. *Gaussian quadrature formulas*. Series in Automatic Computation. Prentice-Hall, Inc, 1966.